Received: 23 December 2022 | Revised: 8 February 2023 | Accepted: 9 April 2023

IET Radar, Sonar & Navigation

DOI: 10.1049/rsn2.12409

The Institution of Engineering and Technology WILEY

ORIGINAL RESEARCH

Fast and precise underwater transducer characterisation utilising adaptive system identification

Bastian Kaulen | **Gerhard Schmidt**

Digital Signal Processing and System Theory, Kiel University, Kiel, Germany

Correspondence
Gerhard Schmidt.
Email: gus@tf.uni-kiel.de

Abstract

Characterising underwater acoustic transducers is essential to optimal signal processing in sound navigation and ranging systems. Precise characterisation allows for equalisation of the input and output hardware, resulting in improved performance of the overall system. A critical quantity of the characterisation is the impulse response of the underwater transducers, which are usually measured in a special low-noise water tank. An established method in other fields to estimate impulse responses of unknown systems is using adaptive filters and include an inherent quality measure. Such approaches allow for very fast and very reliable measurements. However, when using fixed control parameters, a trade-off between convergence speed and final mismatch needs to be found, which can be eliminated using variable control parameters. In this article, a method for determining an optimal step size for adaptive algorithms based on the normalised least mean square method is derived based on a theoretical analysis of the convergence process by taking the reverberation parameters of such measurement tanks into account. The new method is specialised on the application of underwater transducer characterisation and allows a very reliable approximation of the optimal step size and thus a maximally fast adaption behaviour—leading to a very short measurement time. This is firstly shown in simulations and afterwards demonstrated in a real measurement with unknown transducers in a measurement water tank.

KEYWORDS

acoustic measurement, acoustic signal processing, acoustic transducers, adaptive filters, convergence of numerical methods, hydrophones, least mean squares methods, sonar arrays, underwater sound

1 | INTRODUCTION

Acoustic sound waves are the most widely used form of transmitting signals under water in long-range applications [1, 2]. Both for underwater communication and localisation of underwater objects utilising sound navigation and ranging (SONAR) systems [3–5], signals in the form of acoustic waves are transduced into the water by projectors. In the underwater channel, these waves propagate, are eventually reflected by objects, and are finally picked up by hydrophones. Afterwards, depending on the application, such as SONAR or underwater communication, interesting information can be extracted with the help of digital signal processing. It is important to classify all measurable influences as precisely as possible to optimise the performance of signal processing blocks such as beamformers and matched filters. One of the most significant influences that can be measured beforehand is the frequency response of the projectors and hydrophones.

For the characterisation of transducers often, special tanks filled with water in a quiet lab environment are used. On the one hand, such tanks are equipped with sound-absorbing materials mounted on the tank walls to reduce wall and ground reflection. On the other hand, the tanks themselves are mounted on special damping elements to reduce structure-born sound from the rest of the building or environment [6, 7]. Despite these efforts, the limited spatial extent of such

tanks results in a non-neglectable amount of reflections (reverberation) that interfere with the measurements and, therefore, should be reduced by the measurement procedures as much as possible [8].

Classical methods often use short signals to separate the direct sound from the reflections when characterising transducers [6]. However, this has two significant drawbacks. First, it requires a large number of averaging pings to achieve a high signal-to-noise ratio (SNR). In addition, the time between two signal emissions must be long enough during the averaging process that the acoustic energy resulting from the tank reflections has completely decayed. Second, only limited frequency resolution can be achieved due to the short duration of the signals. Especially the first point is a big problem when measuring arrays and thus many transducers because the loop over all transducers (at least the projectors) extends the measurement time even further. This problem increases even more, when directivity patterns are measured since the measurements must be performed over various angles.

An extension that uses longer transmit signals is presented in ref. [9]. Here, a procedure is described that estimates the impulse responses of the system through a deconvolution approach. Thereby the (complex) spectra of the transmit and receive signal are divided, and the impulse response is determined by the inverse Fourier transform of the complex fraction. This method also has the disadvantage of requiring averaging for better precision. The frequency resolution, however, can be better because longer transmit signals can be used. Similar procedures for determining the impulse response are described in refs. [10, 11].

A new method presented in ref. [12] describes the estimation of the impulse response of the system using an adaptive filter. This has the advantage that, on the one hand, the excitation signal can be broadband and, on the other hand, can be transmitted continuously. This way, the measurement time per transducer can be reduced significantly, and the frequency resolution can be increased almost arbitrarily. Another advantage is that the precision of the estimated impulse responses by adaptive algorithms is not limited by the noise floor of the system [13]. Although the adaptation speed decreases with higher background noise, this method is still significantly faster than averaging over several pings due to continuous transmission. Additionally, adaptive algorithms have an inherent quality measure utilising, for example, the error signal. This signal can be used to evaluate the current estimate and to stop the measurement when a desired quality is reached to achieve the minimum measurement time.

The measurement of the impulse response between a projector and a hydrophone is the classical application of system identification using adaptive filter structures. Since the excitation signal is usually very broadband (e.g. white noise), simple (in the sense of required numerical complexity) gradient estimation algorithms such as the normalised least mean square (NLMS) algorithm are used. With such algorithms the system can be identified in real-time [13–15]. In the simplest case, this is controlled by a fixed step size that determines the adaptation speed and the so-called steady-state performance (that determines the final quality of the estimation). However, a variable step size can often achieve much better performance with respect to both of these quantities [16–20]. This publication presents a novel method for determining an adaptive step size control in an optimal manner, which uses the theoretical behaviour of time-invariant systems. This reduces the error between the unknown and the estimated system with maximum speed. For this purpose, a signal model is derived based on assumptions that are especially suitable for measuring transducers in water tanks. The resulting step size control was tested in simulations and confirmed by real measurements.

First, a conventional signal model is introduced and described, followed by a brief explanation of the general NLMS algorithm and the definition of the optimal (time-variant) step size. Subsequently, two derivations for estimating the undisturbed error are given. Then, the theoretical behaviour of the so-called undisturbed error power is shown using a contraction-expansion approach (CEA). For this purpose, simulations compare the performance of the proposed algorithm with the fixed and optimal NLMS. Afterwards, actual measurements are shown, and the quality of the estimates is evaluated. Finally, the results are summarised, and an outlook on possible fields of application is given.

2 | BASICS

2.1 | Measurement environment

The measurements for the NLMS algorithm presented here were carried out in the measuring tank of the Wehrtechnische Dienststelle 71 (WTD 71) of the German Bundeswehr on the site of the Navy Arsenal in Kiel, Germany. It is a 5 m × 5 m tank with a water depth of 3 m and depicted in Figure 1. The used projector array under test can be seen in the right part of the picture. The reference hydrophone Reson TC4014-5 of the company Teledyne Marine [21] is visible on the left and marked with a white circle for a better perceptibility.

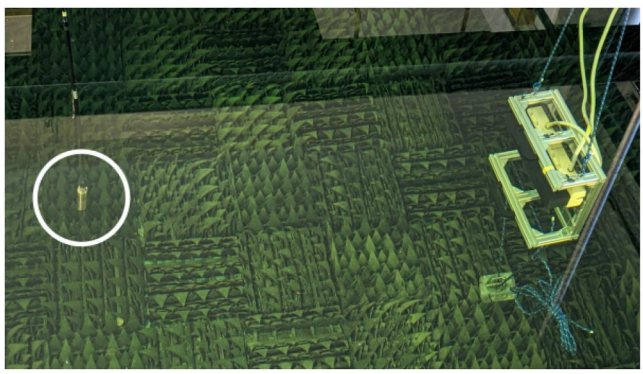

FIGURE 1 Measurement tank of the Wehrtechnische Dienststelle 71 of the German Bundeswehr on the site of the Navy Arsenal in Kiel, Germany. On the left the reference hydrophone is marked with the white circle. On the right the projector array under test is visible.

A typical impulse response is shown in Figure 2. It was measured with an adaptive filter but without using the variable step size control presented in the next sections. The first big impulse at around 2 ms is the direct blast, which contains the desired information of the frequency responses of the projector as well as the hydrophone. Due to the geometrical positions of the projectors and hydrophones and the assumption that no signal can travel through the water faster than the speed of sound, the direct blast can be assumed to be the first signal that will arrive at the hydrophones. With a given sound velocity of $c_w \approx 1500\ \frac{m}{s}$ the distance between projector and hydrophone can be calculated to be around 3 m which aligns well with the geometric distances of the setup. After the direct blast, a few reflections are visible, for example, from the tank's surface and bottom. A more detailed analysis of a long impulse response will be given later in Sec. 3.1.

Since the frequency response of the unknown transducer (projector or hydrophone) cannot be measured independently, the entire *chain* must be analysed within such measurements, which includes the digital-analog-converter (DAC), the projector, the underwater channel itself, the hydrophone and the analog-digital-converter (ADC). By using a so-called *reference channel approach* (meaning the excitation signal output of the DAC is directly connected with the ADC, in addition to the connection to the amplifier of the projector) and assuming that all transmit and receive channels have the same electrical properties, the influence of the AD- and DA-converters can be completely removed. Another important assumption for this approach is that the ADC and DAC are broadband to not influence the excitation signal $\boldsymbol{x}(n)$. Also, using a fully known reference hydrophone or projector, the frequency response can be removed from the unknown transducer estimate. The impulse response can be used to remove the influences of the underwater channel, and the direct sound can be *cut out*. This removes any reflections from the measurement tank. A detailed description of this method is given in [12].

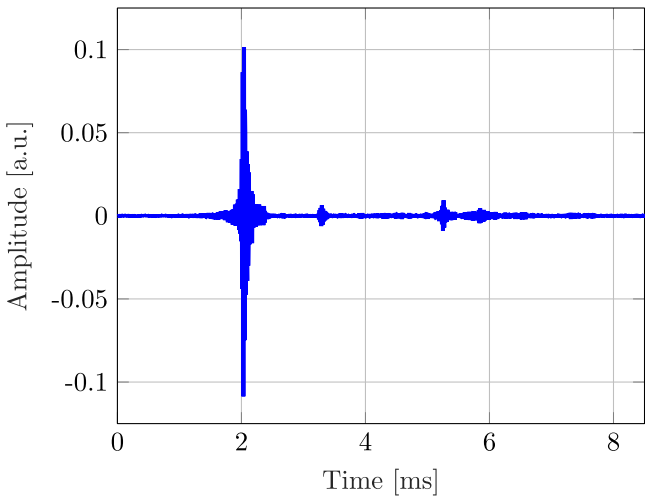

FIGURE 2 Typical impulse response of the presented measurement tank, which shows the direct blast at around 2 ms and the reflections from the surface and the walls afterwards.

2.2 | Conventional system model

The classic model for system identification is shown in Figure 3. Here, for the reason of simplicity, all AD and DA converters are omitted and all models are described completely in the discrete domain.

It consists of an adaptive filter connected in parallel to an unknown system. The known excitation signal $x(n)$ is transmitted into both systems. The last N samples form the excitation vector

$$\boldsymbol{x}(n) = [x_0(n), x_1(n), \ldots, x_{N-1}(n)]^{\mathrm{T}}. \tag{1}$$

The output of the desired system is called $d(n)$ and is given by

$$d(n) = \boldsymbol{h}^{\mathrm{T}}\ \boldsymbol{x}(n), \tag{2}$$

where $\boldsymbol{h}$ represents the unknown system's impulse response with length N. Both the unknown system as well as the estimated system are assumed to be modelled by finite-impulse-response (FIR) filters (FIR filters) and with the coefficient vectors being defined as

$$\boldsymbol{h} = [h_0,\ h_1,\ \ldots,\ h_{N-1}]^{\mathrm{T}} \tag{3}$$

and

$$\hat{\boldsymbol{h}}(n) = \left[\hat{h}_0(n),\ \hat{h}_1(n),\ \ldots,\ \hat{h}_{N-1}(n)\right]^{\mathrm{T}}, \tag{4}$$

respectively. Similar to the unknown system, the output of the adaptive filter is obtained by convolving the excitation signal with the estimated impulse response $\hat{\boldsymbol{h}}(n)$ in terms of

$$\hat{d}(n) = \hat{\boldsymbol{h}}^{\mathrm{T}}(n)\ \boldsymbol{x}(n). \tag{5}$$

Since actual measurements in practice are always superimposed with noise, a noise term $w(n)$ is added to the output signal $d(n)$ and therefore forms the actual measured signal $y(n)$. The difference between this measured input signal $y(n)$ and the estimated output signal $\hat{d}(n)$ is called the error signal $e(n)$ and can be calculated as

$$e(n) = y(n) - \hat{d}(n), \tag{6}$$

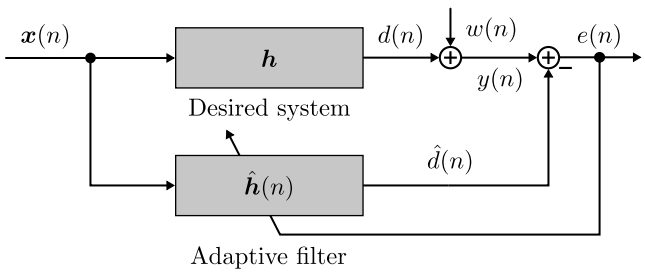

FIGURE 3 Adaptive filter model for system identification.

$$= d(n) + w(n) - \hat{d}(n). \tag{7}$$

2.3 | NLMS-algorithm

The NLMS algorithm is a numerically robust and efficient algorithm often used for system identification. It applies a gradient-based correction to minimise the mean square error between two signals. Depending on the application of the algorithm, one can identify or equalise systems. A detailed derivation is omitted here, and reference is made to [13]. The signal flow according to Figure 3 was chosen in the form of system identification.

Thus, the equations for the NLMS algorithm for estimating an unknown system $\boldsymbol{h}(n)$ with the transmitted signal $\boldsymbol{x}(n)$ are [13]:

$$\hat{d}(n) = \hat{\boldsymbol{h}}^{\mathrm{T}}(n)\ \boldsymbol{x}(n) \tag{8}$$

$$e(n) = y(n) - \hat{d}(n) \tag{9}$$

$$\|\boldsymbol{x}(n)\|^2 = \|\boldsymbol{x}(n-1)\|^2 - x^2(n-N) + x^2(n) \tag{10}$$

$$\hat{\boldsymbol{h}}(n+1) = \hat{\boldsymbol{h}}(n) + \mu\ \frac{\boldsymbol{x}(n)\ e(n)}{\|\boldsymbol{x}(n)\|^2}. \tag{11}$$

Equation (10) describes the recursive update of the squared norm of the excitation vector $\boldsymbol{x}(n)$ for which an efficient and robust method of calculation is given by [22]. Finally, Equation (11) computes the new estimate of the system $\hat{\boldsymbol{h}}(n)$ based on the current input for the time step $n+1$. The parameter μ describes the update's step size and controls the algorithm's convergence. In Equation (11), this step size was chosen to be constant to display the most basic approach of the NLMS algorithm. In the following, a method to calculate a time-variable step size $\mu(n)$ is shown, which is a close estimate for the optimal step size, yielding the fastest convergence and smallest system mismatch.

The NLMS algorithm has been discussed in many publications and customised for specific applications. The book [13] is mentioned here since it provides the derivations for many of the equations used. Furthermore, the publication [17] should be noted, which presents an efficient method for determining a variable step size in the form of the nonparametric variable step size NLMS (NPVSS-NLMS). It was developed specifically with the ambition of non-stationary systems, which does not occur in the measurement application presented here. An advanced step size control was addressed in the publication [20] in the form of the joint-optimised NLMS (JO-NLMS), which will result in a similar solution to the method proposed here, but is derived differently with slightly other assumptions. Furthermore, it does not include influences of the remaining impulse responses present in the form of reverberation of measurement tanks. A summary of the NPVSS-NLMS and the JO-NLMS is provided in the publication [19]. In it, the derivations and the results of the different algorithms for applying acoustic echo cancellation are compared.

3 | PROPOSED ALGORITHM

3.1 | Extended impulse response

To derive the proposed algorithm, an analysis of a system with a long impulse response (longer than the one of the adaptive filter) is presented. In *classic* system identifications, the impulse response of the desired (unknown) system is modelled as an FIR filter with a limited length N that is the same as the adaptive filter. In reality, however, the impulse responses of water measurement tanks are often much longer than the lengths of used adaptive filters. This is caused by the reflections of the excitation signal at the walls in the tank and is a problem often analysed in air acoustics [23]. Through absorption at surfaces, this energy decreases over time until it finally falls below the bground noise and can be neglected. This energy decay decreases exponentially over time and is often referred to as T_{60} time, which describes the decay in power of 60 dB in the impulse response [24]. The general concept also applies to underwater sound and measuring tanks since it is an acoustic phenomenon [7, 8].

Figure 4 shows a typical impulse response of a water tank between a projector and hydrophone on a logarithmic scale. A particularly high filter length of $N_{\mathrm{long}} = 7500$ samples or $T_{\mathrm{long}} = 39.06$ ms at a samplerate of $f_s = 192$ kHz, was chosen for this measurement to illustrate both the influences of the remaining system and the background noise in the impulse response. The blue line corresponds to the long impulse response $h^2_{i,\mathrm{long}}$. The black line in Figure 4 describes the smoothed variant for a better visualisation. The coloured areas represent different sections of the impulse response described in the following.

The green area colourizes the impulse response to be estimated later by applying the NLMS algorithm. In the

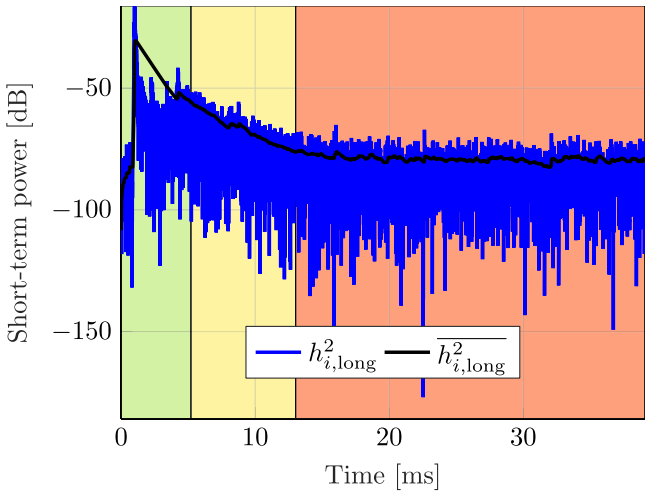

FIGURE 4 Original long impulse response $h^2_{i,\mathrm{long}}$ in blue and smoothed long impulse response $\overline{h^2_{i,\mathrm{long}}}$ in black.

schematic Figure 3, this corresponds to the system $\boldsymbol{h}$ and was later chosen to have a length $N = 1500$ samples. The minimum length N is chosen based on the distance between the projector and the hydrophone. For the given measurement setup, it is about 3 m between projector and hydrophone, this corresponds to around 2 ms or around 384 samples. N should be selected longer, though, because the reflections' energy is, for this reason, modelled in the adaptive filter and will reduce the error signal $e(n)$.

The second (yellow) region represents the system's exponentially decaying remaining impulse response. This arises from reflections of the excitation signal from walls, the water surface, and the ground. The power of this region is thus directly dependent on the power of the excitation signal $\boldsymbol{x}$ and is later used for a comprehensive estimation of involved noise processes.

The red region is a noise plateau formed by the background noise in the overall system. This is determined by its power σ_b^2 and thus also forms a lower limit for the power of the received signal $y(n)$.

3.2 | Artificial impulse response

At this point, an arbitrary long impulse could be generated and used in simulations. However, to keep the simulation as similar as possible to the real application of transducer characterisation in underwater measurement tanks, a theoretical artificial long impulse is derived in the following. The signal power caused by the remaining system $\boldsymbol{h}_{\text{rem}}$ needs to be estimated to form a better model. The artificial impulse response is based on the long impulse response from Figure 4. It extends it by introducing knowledge and assumptions about the general behaviour of acoustic decay in reverberate rooms. To neglect the background noise of the specific measurement of the long impulse response, which power was around −75 dB, the decay parameters can be estimated from the decay region, depicted in the yellow area. To get a more robust estimation of the starting and end value, the smoothed squared long impulse $\overline{\boldsymbol{h}^2_{\text{long}}}$ was used as a base. The gradient

$$f_{\text{grad}} = \frac{\overline{h^2_{\text{long},\kappa_{\text{des,end}}}} - \overline{h^2_{\text{long},\kappa_{\text{des,beg}}}}}{\kappa_{\text{des,end}} - \kappa_{\text{des,beg}}} \tag{12}$$

was calculated by dividing the difference between the decay ending point $\overline{h^2_{\text{long},\kappa_{\text{des,end}}}}$ and the decay starting point $\overline{h^2_{\text{long},\kappa_{\text{des,beg}}}}$ by the difference of samples between those points indexed by $\kappa_{\text{des,end}}$ and $\kappa_{\text{des,beg}}$ respectively. Therefore, the gradient f_{grad} describes the estimated average decay per sample. In order to remove the influence of the noise floor from the measured long impulse response, the rear area marked in red will be replaced. The artificial impulse response is therefore created by

$$h_{\text{art},\kappa} = \begin{cases} h_{\text{long},\kappa} & , \text{for } \kappa > \kappa_{\text{des,end}}, \\ u(\kappa)\, f_{\text{grad}}^{\kappa} \sqrt{\overline{h^2_{\text{long},\kappa_{\text{des,end}}}}} & , \text{for } \kappa \le \kappa_{\text{des,end}}, \end{cases} \tag{13}$$

where $u(\kappa)$ is a random variable generated from a normal distribution. The resulting artificial impulse response is shown in Figure 5.

3.3 | Extended model

To derive the novel approach of this paper, the simple signal model presented in Sec. 2.2 is extended as a first step. This is illustrated in Figure 6 and since it is based on the simpler model depicted in Sec. 3, only the modifications and extensions are presented below.

The first extension includes taking into account possible longer impulse responses, which are described in more detail in Sec. 3.1. This represents a version closer to the truth since, in reality, impulse response decay duration is often significantly longer than the length N of the adaptive filter. Because this remaining part of the impulse response $\boldsymbol{h}_{\text{rem}}$ represents only

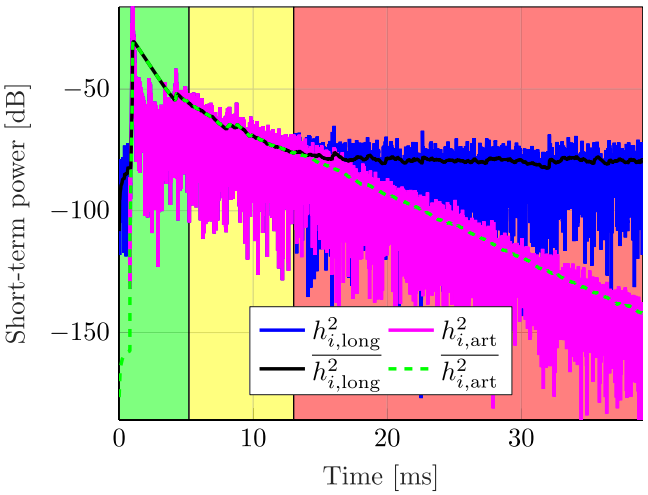

FIGURE 5 Original long impulse response $h^2_{i,\text{long}}$ in blue, smoothed long impulse response $\overline{h^2_{i,\text{long}}}$ in black, artificial impulse response $h^2_{i,\text{art}}$ in magenta and smoothed artificial impulse response $\overline{h^2_{i,\text{art}}}$ in green.

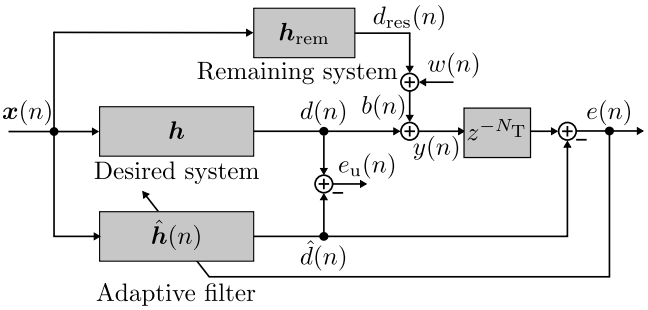

FIGURE 6 Extended adaptive filter model for system identification.

the remaining segment of the total impulse response, it is delayed by N cycles. The result of the convolution between remaining impulse response $\boldsymbol{h}_{\text{rem}}$ and the delayed excitation signal $\boldsymbol{x}_{\text{rem}}(n)$, therefore given by

$$d_{\text{rem}}(n) = \boldsymbol{h}_{\text{rem}}^{\text{T}}\ \boldsymbol{x}_{\text{rem}}(n) \tag{14}$$

and called the remaining output signal $d_{\text{rem}}(n)$. The delayed excitation vector is created similar to the one defined in Equation (1), but filled with delayed excitation signal samples, and the length is chosen to match with $\boldsymbol{h}_{\text{rem}}$. It should be noted that the power of this signal is directly coupled to the excitation power σ_x^2. The resulting signal can be interpreted as an additional noise term and is added to the measurement noise $w(n)$ to form the total noise signal $b(n)$ in the form of

$$b(n) = \hat{\boldsymbol{h}}_{\text{rem}}^{\text{T}}\ \boldsymbol{x}_{\text{rem}}(n) + w(n). \tag{15}$$

As in the simple model, the sum of the undisturbed output signal $d(n)$ and the noise signal $b(n)$ is given by

$$y(n) = d(n) + d_{\text{rem}}(n) + w(n) \tag{16}$$

$$= d(n) + b(n) \tag{17}$$

and forms the measurement signal $y(n)$.

The second extension involves introducing the undisturbed error signal $e_u(n)$. It is the difference between the undisturbed output signal $d(n)$ and the estimated output signal $\hat{d}(n)$ through

$$e_{\text{u}}(n) = d(n) - \hat{d}(n). \tag{18}$$

By inserting Equations (2) and (8) into Equation (18)

$$e_{\text{u}}(n) = \boldsymbol{h}^{\text{T}}\ \boldsymbol{x}(n) - \hat{\boldsymbol{h}}^{\text{T}}(n)\ \boldsymbol{x}(n) \tag{19}$$

is obtained. Furthermore, the difference between the unknown system $\boldsymbol{h}$ and the estimated system $\hat{\boldsymbol{h}}(n)$

$$\boldsymbol{h}_{\Delta}(n) = \boldsymbol{h} - \hat{\boldsymbol{h}}(n). \tag{20}$$

forms the so-called *system mismatch vector* $\boldsymbol{h}_{\Delta}(n)$. The expectation of its squared norm is called *system distance* $\text{E}\{\|\boldsymbol{h}_{\Delta}(n)\|^2\}$ and provides a direct measure for evaluating the estimation. It should be noted that this parameter is only available in simulations because the undisturbed output signal $d(n)$ can not be measured directly.

3.4 | Variable step size

An extension of the classic NLMS algorithm is a *variable step size*, which can be chosen for each time step individually. A *fixed step size* forces a trade-off between convergence speed and final system mismatch. Such attempts lead to a non-optimal convergence in terms of speed or final mismatch of the estimated system. A variable step size with an optimally chosen value for each time step will lead to a continuously improving system distance with the fastest convergence speed.

In [13], a definition of the optimal step size given, but requires two assumptions to be fulfilled.

- The first one needs the squared norm of the excitation signal $\|\boldsymbol{x}(n)\|^2$ to be approximable by a constant, which is fulfilled since the excitation signal is assumed to be stationary white noise.
- The second assumption states that the excitation vector $\boldsymbol{x}(n)$ and the noise signal $b(n)$ need to be orthogonal.

Because the noise signal $b(n)$ consists of the additive noise $w(n)$ (uncorrelated with the excitation) and the remaining output signal $d_{\text{rem}}(n)$ and latter is the convolution between $\boldsymbol{x}(n)$ and $\boldsymbol{h}_{\text{rem}}$ as shown in Equation (15), the noise contains partially the excitation signal $x(n)$. Nevertheless, because this signal is delayed by N samples and assumed to be white, the assumptions of orthogonality still hold.

Since both requirements are true, the optimal variable step size $\mu_{\text{opt}}(n)$ is given by [13] through

$$\mu_{\text{opt}}(n) = \frac{\text{E}\{e_{\text{u}}^2(n)\}}{\text{E}\{e^2(n)\}}. \tag{21}$$

Equation (21) requires both the short-term power of the undisturbed error $e_u(n)$ and the error $e(n)$. The latter is a known signal since it is calculated directly in the classical NLMS Equations (8–11). The undisturbed error $e_u(n)$, on the other hand, is not measurable in real applications since it represents the error between the estimated output signal $\hat{d}(n)$ and the real output signal $d(n)$. In the following, two approaches for estimating the undisturbed error, respectively its short-term power, are derived.

3.5 | Method A: undisturbed error estimation

In real applications, the signal $d(n)$ is superimposed on the one hand with additive noise $w(n)$ and on the other hand with the output signal $d_{\text{rem}}(n)$ resulting in the signal $y(n)$ as stated in Equation (16). To get an estimate of the expected value of the undisturbed error power $\text{E}\{e_{\text{u}}^2(n)\}$ the power of noise signal σ_{b}^2 can be used.

When assuming a stationary system, the noise power σ_{b}^2 can be calculated by subtracting the powers of the containing signals. By looking at Figure 6 and according to the Equations (6) and (16), the error signal $e(n)$ is composed of the undisturbed error $e_u(n)$ and the noise $b(n)$. Under the assumption of white noise, the estimated value of the undisturbed error signal can now be calculated by

$$\begin{aligned}
\mathrm{E}\{e_{\mathrm{u}}^2(n)\} &= \mathrm{E}\{e^2(n)\} - \mathrm{E}\{b^2(n)\},\\
&= \mathrm{E}\{e^2(n)\} - \sigma_w^2 - \mathrm{E}\{d_{\mathrm{rem}}^2(n)\},\\
&= \mathrm{E}\{e^2(n)\} - \sigma_w^2 - \mathrm{E}\{(\boldsymbol{x}_{\mathrm{rem}}^{\mathrm{T}}(n)\ \boldsymbol{h}_{\mathrm{rem}})^2\},\\
&= \mathrm{E}\{e^2(n)\} - \sigma_w^2 - \sigma_x^2\ \mathrm{E}\{\boldsymbol{h}_{\mathrm{rem}}^{\mathrm{T}}\ \boldsymbol{h}_{\mathrm{rem}}\},\\
&= \mathrm{E}\{e^2(n)\} - \sigma_w^2 - \sigma_x^2 \sum_{i=0}^{\infty} h_{\mathrm{rem},i}^2\\
&= \mathrm{E}\{e^2(n)\} - \sigma_w^2 - \sigma_x^2 \sum_{i=N}^{\infty} h_i^2.
\end{aligned} \tag{22}$$

In practice, however, this method did not provide satisfying results. It showed problems when the estimated undisturbed error $e_u(n)$ gets smaller than the error signal $e(n)$ itself (in terms of short-term powers). The method required a lot of fine-tuning with different smoothing parameters and was very customised for the specific measurement tank. Therefore, this variant of calculating the undisturbed error was discarded.

3.6 | Method B: contraction-expansion approach

Since the direct method for estimating the short-term power of the undisturbed error has proven to be difficult, another approach is the CEA presented in the following. It is based on the theoretical adaptation behaviour of the NLMS algorithm for stationary systems. It describes the prediction of the system distance based on the previous system distance, the excitation signal power, and the noise power. This approach comprises two terms derived in detail in ref. [13]. The original publication investigated two types of adaption control mechanisms in form of the step size μ and the regularisation $\boldsymbol{\Delta}$. In themselves, both parameters have slightly different properties but can be transformed into each other as described in ref. [13]. In the following, the influence of the regularisation is therefore neglected, resulting in $\boldsymbol{\Delta} = 0$. The first term $A(\mu, N)$ is given by ref. [13] through

$$A(\mu, N) = 1 + \frac{\mu^2}{N} - \frac{2\mu}{N}. \tag{23}$$

It is called the *contraction* parameter and describes the adaptation behaviour of the algorithm in the noise-free case. It ranges from zero to one and represents the system distance decay when the noise power σ_b^2 is zero and, therefore, the dominating part in predicting the next system distance.

The second term $B(\mu, N)$ is described after ref. [13] by

$$B(\mu, N) = \frac{\mu^2}{N} \tag{24}$$

and expresses the influence of the noise $b(n)$. It is called the *expansion* parameter because it counteracts the contraction parameter A (μ, N) by increasing the resulting system distance.

Both terms depend on the filter length N and the chosen step size μ. The filter length N is known beforehand, and the step size μ will be calculated for each time step in the following. The contraction and expansion parameters together with

$$\mathrm{E}\{\|\boldsymbol{h}_{\Delta}(n+1)\|^2\} \approx A(\mu, N)\ \mathrm{E}\{\|\boldsymbol{h}_{\Delta}(n)\|^2\} + B(\mu, N)\ \frac{\sigma_b^2}{\sigma_x^2} \tag{25}$$

form the update function for the approximation of the system distance in the next time step $n + 1$. This update function depends on the current system distance $\mathrm{E}\{\|\boldsymbol{h}_{\Delta}(n)\|^2\}$, the power of the excitation signal σ_x^2, and the noise power σ_b^2. Since the excitation signal $x(n)$ is known, the power of it σ_x^2 can be calculated. The noise power σ_b^2 consists, as stated in Equation (16), of the remaining output signal $d_{\mathrm{rem}}(n)$ and the additive noise term $w(n)$. However, assuming stationarity, the latter can be measured before the actual start of the measurement and averaged over a sufficiently long time. Since the output signal $d_{\mathrm{rem}}(n)$ depends on the excitation signal, which is known, the last unknown quantity is the remaining impulse response $\boldsymbol{h}_{\mathrm{rem}}$. This parameter represents a constant of the measurement tank, which must be measured once for each tank, but should not change afterwards. The exact determination of this parameter is given in the subsequent section. In ref. [13], it is confirmed by simulations that the Formula (25) represents the approximation of the system distance.

In the next step, the system distance $\mathrm{E}\{\|\boldsymbol{h}_{\Delta}(n)\|^2\}$ can be derived from the estimated undisturbed error $\mathrm{E}\{e_{\mathrm{u}}^2(n)\}$ by inserting Equation (18):

$$\begin{aligned}
\mathrm{E}\{e_{\mathrm{u}}^2(n)\} &= \mathrm{E}\left\{\left(d(n) - \hat{d}(n)\right)^2\right\}\\
&= \mathrm{E}\left\{\left(\boldsymbol{x}^{\mathrm{T}}(n)\ \boldsymbol{h} - \boldsymbol{x}^{\mathrm{T}}(n)\ \hat{\boldsymbol{h}}(n)\right)^2\right\}\\
&= \mathrm{E}\left\{\left(\boldsymbol{x}^{\mathrm{T}}(n)\ \boldsymbol{h}_{\Delta}(n)\right)^2\right\}\\
&= \sigma_x^2\ \mathrm{E}\{\|\boldsymbol{h}_{\Delta}(n)\|^2\}.
\end{aligned} \tag{26}$$

After inserting Equation (25) into the previous derived Equation (26), the optimal step size can be calculated each time step in the form of

$$\hat{\mu}_{\mathrm{opt}}(n) = \frac{\sigma_x^2\ \mathrm{E}\{\|\boldsymbol{h}_{\Delta}(n)\|^2\}}{\mathrm{E}\{e^2(n)\}}. \tag{27}$$

The resulting estimation of the optimal step size first requires estimating the system distance. Afterwards, a new estimate of the short-term power of the undisturbed error is calculated every time step, and thus a new step size $\mu(n)$ is calculated that no longer depends on measured inputs.

Due to the iterative nature of this approach, a first initial guess of the system distance needs to be known. For that reason, an artificial delay can be used to estimate the system distance. The idea behind this delay is that it is a known constant of N_Γ samples, in which the system's impulse response is known to be zero. With that assumption, the power of the first N_Γ impulse response samples can be used to estimate the overall system distance. This concept was first proposed in ref. [25] and further refined in ref. [26] and is often used in acoustic echo cancellation [16].

The initial estimate of the system distance can be calculated through the summation of the first N_Γ squared values of the estimated impulse response $\hat{h}$ like

$$\mathrm{E}\left\{\|\boldsymbol{h}_\Delta(n)\|^2\right\}_{\text{init}} = \frac{N}{N_\Gamma} \sum_{i=0}^{N_\Gamma-1} \hat{h}_i^2(n). \tag{28}$$

The sum needs to be multiplied with the correction factor $\frac{N}{N_\Gamma}$ to scale the initial estimate of the system distance with the length of the estimated impulse response proportionally.

The downside of using such an artificial delay is the higher complexity that is introduced. The adaption of the N_Γ samples in the estimated impulse response have no benefit for estimating the actual impulse response besides improving the estimation of the optimal step size. However, the increase in computational complexity is relatively small since, usually, much fewer delay coefficients (compared to the length of the adaptive filter) are required.

3.7 | Realisation

In reality, some of the required parameters of the derivation in Sec. 3.6 are unknown and need to be estimated. In the following, the actual realisation of the CEA-NLMS is described, which stands for contraction-expansion approach NLMS.

While the power of the excitation signal σ_x^2 is known, the power of the additive white noise σ_w^2 is not exactly known but can be estimated prior to measuring the devices under test, for example, the SONAR equipment. To measure the noise floor, a variety of possibilities are given in ref. [18]. The chosen variant for this publication is a first-order IIR filter (infinite-impulse-response filter) with a slowly time-variant smoothing parameter $\beta(n)$ in the form of

$$\overline{w^2(n)} = \beta(n)\ \overline{w^2(n-1)} + (1-\beta(n))\ w^2(n). \tag{29}$$

Initially, the method starts with a fast time constant to initialise the estimator and slows the estimation during runtime to reduce the estimation error. In the given measurement setup with a samplerate of $f_s = 192$ kHz described in Sec. 2.1 a useful value of $\beta = 0.999$ was chosen. Finally, the estimation is stopped at time index n_0, and the last estimated value is used as the estimated noise power

$$\hat{\sigma}_w^2 = \overline{w^2(n_0)}. \tag{30}$$

Another parameter that is not necessarily known is the impulse response of the remaining system $\boldsymbol{h}_{\text{rem}}$. This can be estimated via an initialisation measurement for the classification of the environmental properties of the given environment. This measurement only needs to be done once for the given tank, which in our case is the water tank of the WTD 71, described in Sec. 2.1. Since only the power of the real remaining impulse response is required, only an estimation of the scalar σ_{rem}^2 is needed. To get this parameter, a long impulse response needs to be measured. This can be done with an increased filter length of N_{long} as described in Sec. 3.1. The length N_{long} should be long enough to see the noise floor of the given environment to have a sufficient long foundation to extract the t time of the exponential decay. Afterwards the power of the remaining system $\sigma_{d_{\text{rem}}}^2$ can be estimated by the summation of the artificial impulse response $\boldsymbol{h}_{\text{rem}}$ that was generated in Sec. 3.2 with

$$\sigma_{d_{\text{rem}}}^2 = \sigma_x^2 \sum_{i=N}^{N_{\text{long}}-1} h_{\text{rem},i}^2. \tag{31}$$

At the start of the adaption process, the estimated impulse response $\hat{\boldsymbol{h}}(0)$ is initialised with zeros. This means that the first adaption's error $e(n)$ is the input signal $y(n)$ itself. Therefore, a good value as the initial step size is $\mu_{\text{cea}} = 1$. This is chosen until the ratio between the smoothed squared input power $\overline{y^2(n)}$ and the smoothed squared error signal $\overline{e^2(n)}$ is bigger than a certain threshold α. A step size of one provides the fastest convergence in any scenario until the step size is too large. In this implementation, a threshold of $\alpha = -15$ dB was chosen, which was a good compromise between robustness towards noise and fast convergence.

This publication proposes a model-based step size for the cases when the power ratio is larger than the threshold α. Since the real system distance $\mathrm{E}\{\|\boldsymbol{h}_\Delta(n)\|^2\}$ is hidden in actual measurements, the estimated system distance is for now given by the term $\Gamma(n)$. Following this nomenclature, Equation (25) changes in the real implementation to

$$\begin{aligned}\Gamma(n) = {} & A_{\text{cea}}(\mu_{\text{cea}}(n-1), N)\ \Gamma(n-1) \\ & + B_{\text{cea}}(\mu_{\text{cea}}(n-1), N)\ \frac{\hat{\sigma}_b^2}{\sigma_x^2}.\end{aligned} \tag{32}$$

This result can then estimate the current system distance $\Gamma(n)$ and can be used for calculating the expected squared undisturbed error e_{u}^2 like

$$\mathrm{E}\left\{e_{\text{u}}^2(n)\right\} = \sigma_x^2\ \Gamma(n). \tag{33}$$

Finally, the pseudo-optimal time variable step size can be calculated with

$$\mu_{\text{cea}}(n) = \frac{\mathrm{E}\{e_{\text{u}}^2(n)\}}{\mathrm{E}\{e^2(n)\}} = \frac{\sigma_x^2\,\Gamma(n)}{\overline{e^2(n)}} \quad (34)$$

Since the CEA method of calculating the variable step size does not directly rely on the measured error signal, this method has advantages and disadvantages. By the iterative computation of the system distance and the step size, an ever smaller update and, thus, a better estimate for the impulse response is achieved. In contrast to other methods, this has no theoretical limit, like an estimation of the impulse response using a Kalman filter, which is limited by a smoothing parameter β in the state-space approach [15]. In practice, this is often constrained by numerical limitations or by the maximum measurement time. However, this approach is only valid for stationary systems with a good estimation for excitation and noise power, which is given in the proposed scenario of a water measurement tank. The disadvantage of the CEA-NLMS is that in case of a sudden system change, a much too small step size is assumed, and thus the adaptation is no longer optimal. However, if the change is large enough to increase the error signal $e(n)$ above the chosen limit α, the step size is set to 1 and therefore resets the adaptation process and thus adapts again optimally. Table 1 shows the summary of the CEA-NLMS separated in equations for the initialisation and runtime phase.

4 | SIMULATION RESULTS

Several simulations were performed to test the estimate of the undisturbed error power described before and the resulting variable step size, which have the benefit that all signals and properties are fully known. Therefore, the calculations and comparisons of otherwise usually hidden variables such as system distance or the undisturbed error are possible.

First, an actual impulse response between the projector and hydrophone was determined using classical methods and afterwards modified for this simulation. This is presented in Sec. 3.2 and resulted in the artificial impulse response $\boldsymbol{h}_{\text{art}}$ with the length $N_{\text{long}} = 7500$ samples depicted in Figure 5. To get a realistic setup, the different algorithms are calculating a shorter system with the length of $N = 1500$ samples, which also included the delay time of $N_{\text{T}} = 50$ samples for estimating the initial system distance as described in Sec. 3.6. Since the complete impulse response is known in this simulation, the power of the remaining impulse response $\boldsymbol{h}_{\text{rem}}$ was calculated from the artificial impulse response as shown in Equation (31).

To construct the receive signal, an excitation signal $x(n)$ with a duration of 20 s was created using a zero-mean white Gaussian noise generator with power of $\sigma_x^2 = 1$. After generation, this signal was convolved with the generated artificial impulse response described before. Additionally, a white Gaussian noise signal $w(n)$ was added with the power σ_w^2, which was also defining the SNR. For this paper, the definition of SNR was chosen to be

TABLE 1 Summary of CEA-NLMS separated in equations for the Initialisation and runtime phase.

Initialisation:	
Impulse response	$\hat{\boldsymbol{h}}(0) = \boldsymbol{0}$
Noise	$\hat{\sigma}_b^2 = \hat{\sigma}_w^2 + \hat{\sigma}_{d_{\text{rem}}}^2$
Runtime:	
Estimated input signal	$\hat{d}(n) = \hat{\boldsymbol{h}}^{\text{T}}(n)\,\boldsymbol{x}(n)$
Error signal	$e(n) = y(n) - \hat{d}(n)$
Estimated system distance	$\Gamma(n) = \begin{cases} \frac{N}{N_\Gamma} \sum_{i=0}^{N_\Gamma - 1} \hat{h}_i^2(n), & \text{for } \frac{\overline{y^2(n)}}{\overline{e^2(n)}} \le \alpha, \\ A_{\text{cea}}(\mu_{\text{cea}}(n-1), N)\Gamma(n-1) + B_{\text{cea}}(\mu_{\text{cea}}(n-1), N)\,\frac{\hat{\sigma}_b^2}{\sigma_x^2}, & \text{else.} \end{cases}$ with $A_{\text{cea}}(\mu_{\text{cea}}(n-1), N) = 1 + \frac{\mu_{\text{cea}}^2(n-1) - 2\mu_{\text{cea}}(n-1)}{N}$ and $B_{\text{cea}}(\mu_{\text{cea}}(n-1), N) = \frac{\mu_{\text{cea}}^2(n-1)}{N}$
Step size	$\mu_{\text{cea}}(n) = \begin{cases} 1, & \text{for } \frac{\overline{y^2(n)}}{\overline{e^2(n)}} \le \alpha, \\ \min\left\{1, \frac{\sigma_x^2\,\Gamma(n)}{\overline{e^2(n)}}\right\}, & \text{else.} \end{cases}$
Recursive norm	$\|\boldsymbol{x}(n)\|^2 = \|\boldsymbol{x}(n-1)\|^2 - x^2(n-N) + x^2(n)$
Update filter	$\hat{\boldsymbol{h}}(n+1) = \hat{\boldsymbol{h}}(n) + \mu_{\text{cea}}(n)\frac{\boldsymbol{x}(n)e(n)}{\|\boldsymbol{x}(n)\|^2}$

Abbreviation: CEA-NLMS, contraction-expansion approach NLMS.

$$\mathrm{SNR} = \frac{\sigma_y^2}{\sigma_w^2}. \tag{35}$$

Here, it should be noted that the SNR calculated this way could not be directly read in the following figures as the distance between the smoothed received power $\overline{y^2(n)}$ and the smoothed error power $\overline{e^2(n)}$ since the received signal contains additionally the signal $d_{\mathrm{rem}}(n)$ created by the remaining system.

After summation of $d(n)$, $d_{\mathrm{rem}}(n)$ and $w(n)$ the receive signal $y(n)$ was then applied to an NLMS-based adaptive filter with a fixed step size of $\mu_{\mathrm{fix}} = 0.01$ and a NLMS with the new variable step size $\mu_{\mathrm{cea}}(n)$ to get the system estimates $\hat{\boldsymbol{h}}_{\mathrm{fix}}$ and $\hat{\boldsymbol{h}}_{\mathrm{cea}}$ respectively. The fixed step size of 0.01 was chosen, because it is a rather small step size and therefore has a very low system distance, when the convergence process is finally done. This is a requirement since the characterisation of transducers should fulfill a maximum quality and reach this as fast as possible.

To get a fair result, the processing of all adaptive filter structures starts after a *waiting time* of 1 s to let every parameter and estimate (mainly the short-term power estimations) settle for some time.

Because the intended use of this proposed method is a system identification setup in a special measurement environment, two relatively low noise scenarios are presented. At first, the proposed CEA-NLMS is compared with a conventional NLMS with a fixed step size of $\mu_{\mathrm{fix}} = 0.01$, and afterwards, the CEA-NLMS was compared to the theoretical optimal step size. This optimal step size is available since, in the simulations, every parameter is known and allows for directly calculating the undisturbed error signal power $e_u(n)$ and therefore, the optimal step size $\mu_{\mathrm{opt}}(n)$ for each time step.

4.1 | Contraction-expansion approach versus fixed step size

At first, a comparison between the CEA-NLMS and a fixed step size NLMS with a step size of $\mu_{\mathrm{fix}} = 1$ is presented. The selected SNR of 20 dB depicts a realistic noise scenario for the used measurement tank.

The Figure 7 displays the essential signals in the form of their short-term power for illustrating the performance of both NLMS algorithms. The smoothed received signal $\overline{y^2(n)}$ is depicted in red and constant over the whole signal duration. The error signal of both algorithms $\overline{e^2_{\mathrm{fix}}(n)}$ and $\overline{e^2_{\mathrm{cea}}(n)}$ start at the same power as the receive signal because the error signal before the adaption only contains the receive signal itself.

It is visible that both algorithms behave the same at the start of the adaptation process at 0 s. This is due to the fact, that both algorithms use the same step size of 1 in the beginning. Therefore, both the error signals $\overline{e^2_{\mathrm{fix}}(n)}$ and $\overline{e^2_{\mathrm{cea}}(n)}$ as well as the estimated system distances $\overline{\Gamma_{\mathrm{fix}}(n)}$ and $\overline{\Gamma_{\mathrm{cea}}(n)}$ are very similar. This behaviour, however, changes when the difference between the smoothed input power $\overline{y^2(n)}$ and the smoothed error power $\overline{e^2_{\mathrm{cea}}(n)}$ is bigger than α. Now the new method of calculating the step size is used, which decreases μ_{cea} over time, allowing for an improving estimate of the impulse response, which is visible in $\overline{e^2_{\mathrm{u,cea}}(n)}$ and $\overline{\Gamma_{\mathrm{cea}}(n)}$. The fixed step size NLMS can not improve much further than the smoothed error power $\overline{e^2_{\mathrm{fix}}(n)}$ and therefore has an inaccurate estimate of the impulse response. This shows that the chosen step size of $\mu_{\mathrm{fix}} = 1$ is too large since the required precision in estimation is not met.

The second comparison between the CEA-NLMS and a fixed NLMS is discussed with a step size of $\mu_{\mathrm{fix}} = 0.01$, which results in an improved but slower estimate. The selected SNR is again 20 dB.

The first difference in Figure 8 is the behaviour of those error signals after 1 s when the adaptation process starts. It is visible that the error signal $\overline{e^2_{\mathrm{cea}}(n)}$ drops much faster than the error signal $\overline{e^2_{\mathrm{fix}}(n)}$ of the fixed NLMS. The different choices of step size can explain this. The adaptive step size control has a step size of 1 at the beginning of the adaptation process and thus drops the fastest. In contrast, the fixed step size of 0.01 adapts much more slowly. After some time, however, both reach the same lower limit of error power. This is founded on a limit given by the background noise and cannot be underrun by both algorithms when looking only at the error signal itself.

The smoothed system distances $\overline{\Gamma(n)}$ are analysed for the second difference. This quantity indicates the error between the real and the estimated impulse responses accumulated over the total impulse response length. It shows a behaviour similar to the error signals. At first, both start at the power of the receive signal and drop after the adaptation process starts. However, the system distance of the CEA-NLMS falls significantly faster than that of the fixed NLMS. This is also due to the larger step size at the start of the adaptation process. An important observation is the convergence behaviour of the two

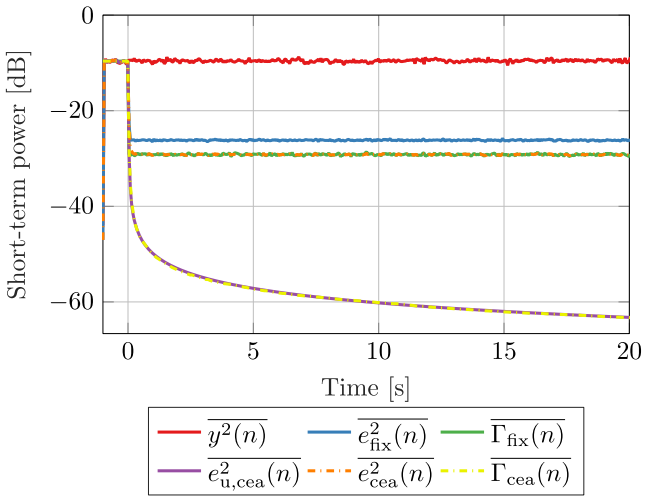

FIGURE 7 Adaptation of the CEA-NLMS compared to a fixed normalised least mean square (NLMS) with a step size of $\mu_{\mathrm{fix}} = 1$ in a signal-to-noise ratio (SNR) of 20 dB for a duration of 20s.

algorithms. The system distance of the fixed NLMS falls more slowly, reaching a plateau of about −52 dB at about 6 s. This is, in the end, limited by the step size and cannot be undershot even with infinite adaptation time. The CEA-NLMS, on the other hand, shows a deceleration of the descent starting at about 4 s but does not reach a plateau. This is due to the constantly decreasing step size, which makes an arbitrarily small system distance possible. A more detailed consideration of the final mismatch is given below in Sec. 4.4.

A third comparison, where only the SNR is changed to 40 dB, is illustrated in Figure 9. The same behaviour can be observed here, with the small difference that both the error signals and the achievable system distance are smaller. Both can be attributed to the better SNR and, thus, the lower noise floor.

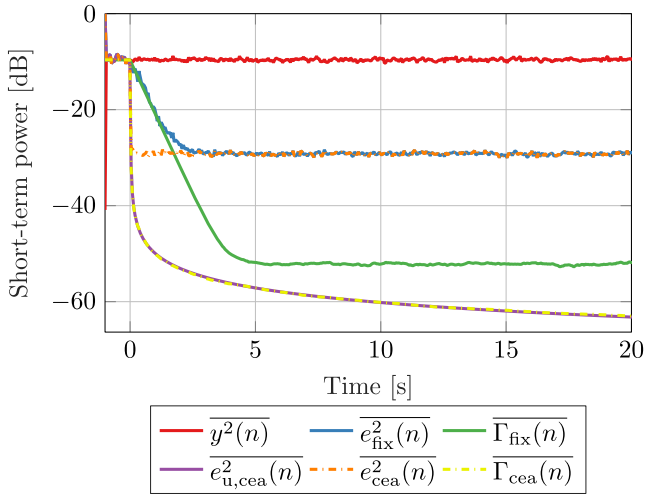

FIGURE 8 Adaptation of the CEA-NLMS compared to a fixed normalised least mean square (NLMS) with a step size of $\mu_{\mathrm{fix}} = 0.01$ in a signal-to-noise ratio (SNR) of 20 dB for a duration of 20 s.

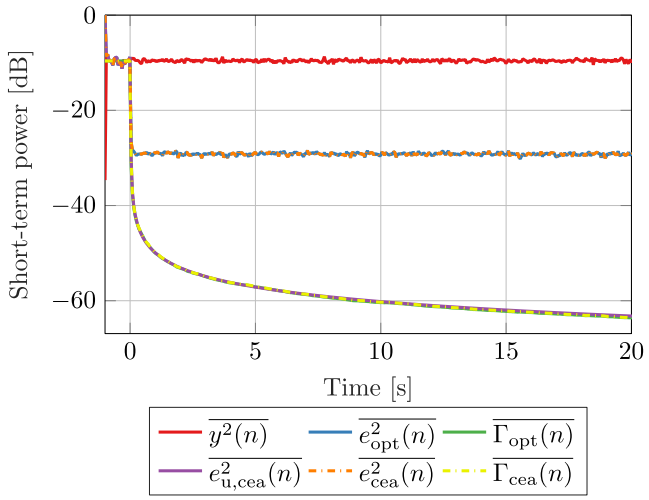

FIGURE 9 Adaptation of the CEA-NLMS compared to a fixed normalised least mean square (NLMS) with a step size of $\mu_{\mathrm{fix}} = 0.01$ in a signal-to-noise ratio (SNR) of 40 dB for a duration of 20 s.

4.2 | contraction-expansion approach versus optimum step size

In addition to the comparison with the fixed NLMS, the comparison of the CEA-NLMS with the optimal step size is also considered below. The optimal step size can be calculated in simulations since the undisturbed error $e_u(n)$ is known in the simulation. After squaring, the smoothed value can be utilised as a very good approximation for the expected value $\mathrm{E}\{e^2_{\mathrm{u}}(n)\}$ and after inserting it into Equation (34), it can be used to calculate the optimal step size $\mu_{\mathrm{opt}}(n)$.

In the figure Figure 10 the adaptation behaviour is shown on the one hand of the CEA-NLMS and the other hand of the optimal VSS-NLMS at an SNR of 20 dB. Here, both the received signal $\overline{y^2(n)}$ and the error signals $\overline{e^2_{\mathrm{opt}}(n)}$ and $\overline{e^2_{\mathrm{cea}}(n)}$ show very similar behaviour as in the previous simulations. Both system distances decrease quickly and lay on top of each other in the plot. This again points out that the presented method in the form of the CEA-NLMS shows an excellent and nearly optimal convergence behaviour.

4.3 | Convergence speed

One of the goals of the CEA-NLMS was to reduce the time per measurement. For this purpose, the convergence speed was shown in Figure 11.

To better compare the convergence speed, an enlarged version of Figure 8 is shown in Figure 11. Here, the range from −0.5 to 4.5 s is shown, which contains the beginning of the adaptation process. It can be seen that the system distance of the CEA-NLMS decreases much faster than that of the fixed NLMS. This can again be easily seen by the dashed red line drawn at −50 dB. The CEA-NLMS reaches it after 1 s, whereas the fixed NLMS only 4 s after the start of adaptation. This speed increase of 3 s does not sound like much as an absolute

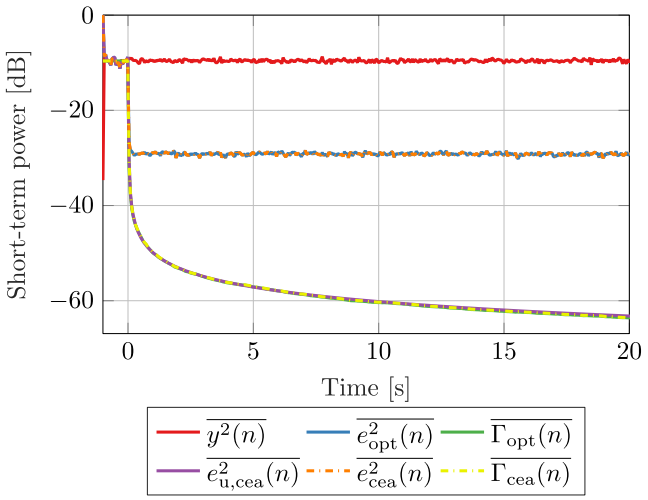

FIGURE 10 Adaptation of the CEA-NLMS compared to an optimal normalised least mean square (NLMS) with a step size $\mu_{\mathrm{opt}}(n)$ in a signal-to-noise ratio (SNR) of 20 dB for a duration of 20 s.

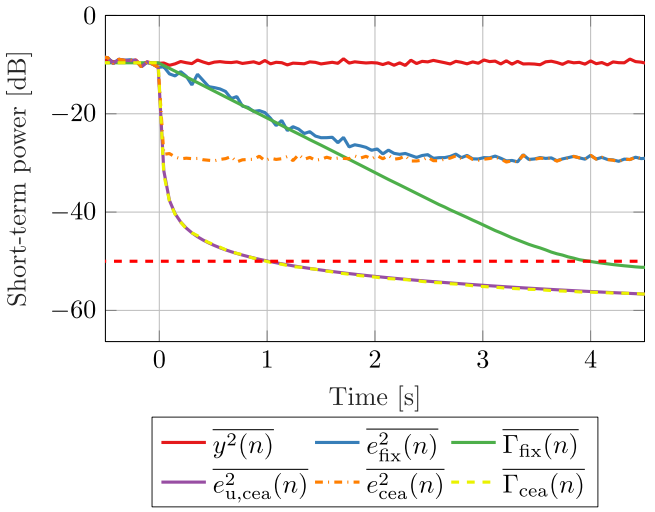

FIGURE 11 Enlarged view of Figure 8 to better illustrate the convergence speed at the beginning of the adaptation process. The system distance of the CEA-NLMS, shown in dashed and yellow, reaches −50 dB after 1 s, whereas the fixed normalised least mean square (NLMS), shown in green, reaches this value after an adaptation time of 4 s.

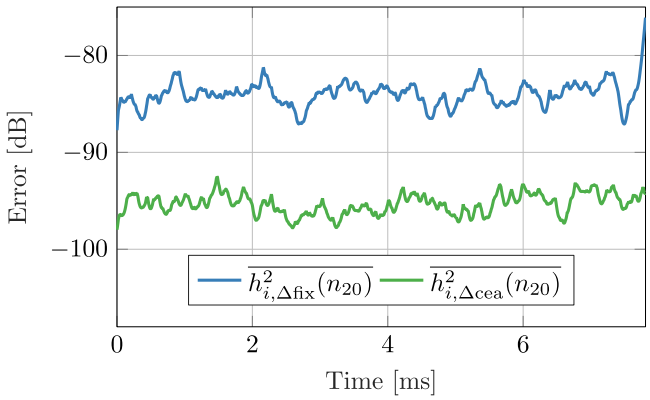

FIGURE 12 Final mismatch after 20 s of adaptation. In blue is the smoothed squared system mismatch vector $\overline{h^2_{i,\Delta\mathrm{fix}}}$ of the fixed normalised least mean square (NLMS), in green is the smoothed squared system mismatch vector $\overline{h^2_{i,\Delta\mathrm{cea}}}$ of the CEA-NLMS depicted. It can be seen that the latter provides an about 10 dB better estimate over the entire impulse response.

value for a single measurement, but if arrays with many different elements are measured in different directions, the measurement time is reduced to a quarter. Datasheets of transducers often include directivity patterns for the horizontal and vertical axes but very rarely with a complete three-dimensional directivity pattern. The reason for this might be the drastically increased measurement time when all axes are characterised. This number of measurements can easily exceed 1200 per element with a rather poor angular resolution of only $\varphi\Delta = 5°$ and $\theta_\Delta = 5°$. However, often chosen angular resolutions, especially around 0° are much finer, which will increase the number of measurements even further. When characterising transducers, the demonstrated reduction by a factor of four using the CEA-NLMS instead of a fixed step size solution is a major improvement.

4.4 | Final mismatch

Besides the fast measurement of projectors and hydrophones, the goal was to obtain a measurement as accurately as possible. This is mainly characterised by the error between real and estimated impulse response in the form of the system mismatch vector $\boldsymbol{h}_\Delta$. As in Sec. 3.3, this describes the error over the entire impulse response length and should be as small as possible.

The Figure 12 shows the smoothed squared final system mismatch vector for both the fixed NLMS and the CEA-NLMS from the simulation in Sec. 4.1 at an SNR of 20 dB. It was taken after the simulation time of 20 s and denoted as n_{20}, which represents the discrete index n at the time 20 s. It can be seen that the CEA-NLMS is about 10 dB better over the entire impulse response, which fulfills the requirement for an accurate measurement.

It should also be mentioned here that with a longer adaptation time, the matching should continuously improve and thus provide a better and better estimate. In practice, however, this is often unnecessary since there is often a sufficient limit. This limit also shows that the NLMS approach for measuring underwater transducers has the advantage of a quality measure. This means that the actual measurement can be evaluated with the error signal and the estimated undisturbed error signal. This is impossible in other methods, for example, by averaging over many short pings.

4.5 | System distance estimation

Since the system distance estimate is an important parameter for the CEA-NLMS, an analysis of the estimation is done in the following. For that, a look at Equation (28) is necessary where the formula for the initial system distance estimate is given by calculating the power of the first N_Γ samples of the impulse response. This procedure ensures a valid initial system distance estimate $\Gamma(n)$ for calculating the CEA step size.

Figure 13 shows the first N_Γ samples, which correspond to 0.8 ms, of the squared estimated impulse response for a fixed NLMS in orange and the CEA-NLMS in purple. It is visible that the difference between both lines is around 10 dB, which indicates the better performance of the CEA-NLMS algorithm. For comparison, the real smoothed squared system distance vector is depicted as dotted lines in blue for the fixed NLMS and green for the CEA-NLMS. On the one hand, both algorithms differ the same as the estimated impulse response. On the other hand, the estimated impulse responses have the same power as the smoothed system distances for the corresponding step size control. The way the parameters were calculated explains their smoothness differences since the system distance is smoothed over multiple time indices. At the same time, the impulse response is a snapshot of the single index and, therefore, noisier.

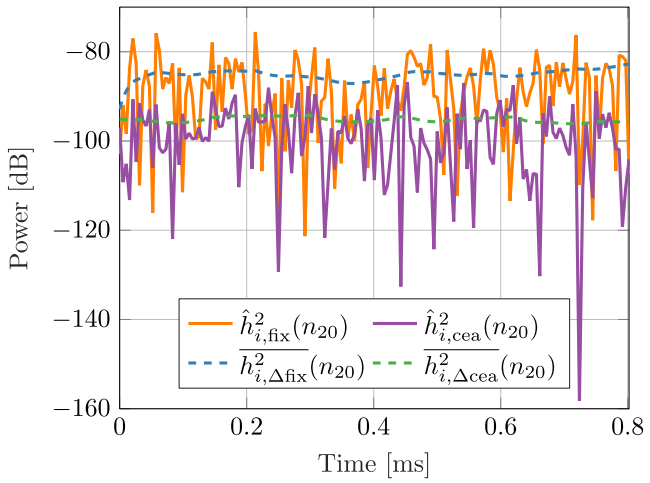

FIGURE 13 First N_T samples of the squared estimated impulse response for a fixed normalised least mean square (NLMS) in orange and the CEA-NLMS in purple. The difference between both is around 10 dB. For comparison, the real smoothed system distance vector for the fixed NLMS in blue and the CEA-NLMS in green show a similar difference and therefore justify the estimate of the system distance.

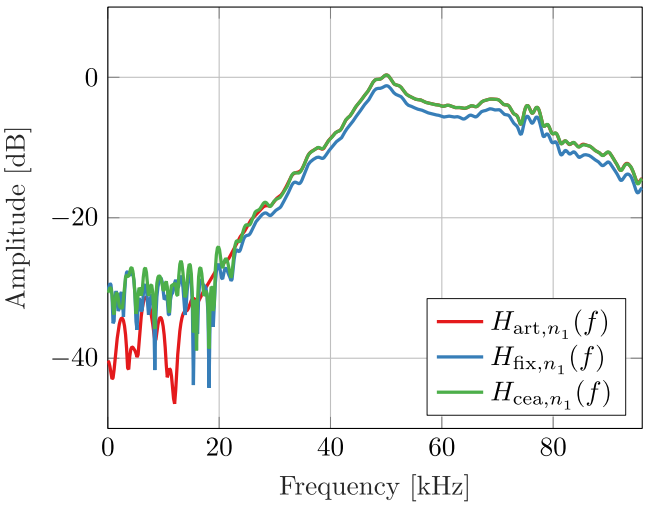

FIGURE 14 Magnitude of the cut direct blast after 1 s of adaption. The magnitude estimated with the proposed contraction-expansion approach (CEA) method (depicted in green) shows no visible difference in the interested frequency range between 40 and 60 kHz in comparison with the original artificial magnitude depicted in red. However, the magnitude estimated with the fixed step size control, depicted in blue, is still adapting and has a bigger error than the CEA method.

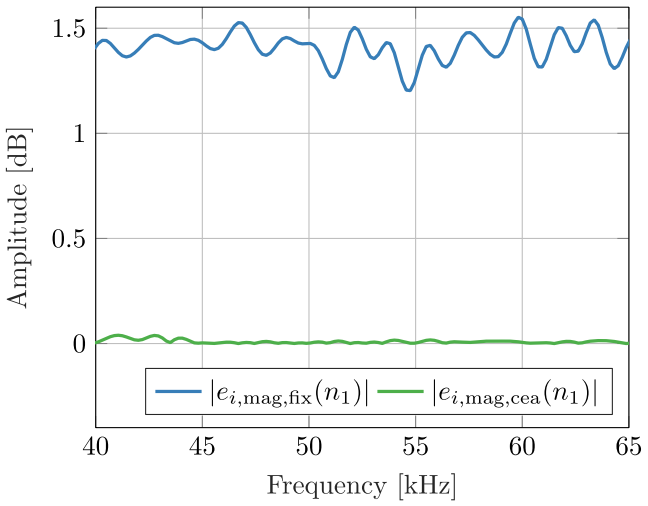

FIGURE 15 Difference in magnitude of the cut direct blast after 1 s of adaption in the interested frequency range between 40 and 60 kHz. The magnitude estimated with the CEA-NLMS (depicted in green) shows a smaller error in comparison to the magnitude estimated with the fixed step size control depicted in blue.

4.6 | Influences in the frequency response

Since the final goal was to propose a fast and precise way of underwater transducer characterisation, the influences in frequency responses in the form of magnitudes and group delays are presented. For that the direct blast of the calculated impulse responses was cut out and transferred via a Fourier transformation in the frequency domain. This concept is further described in the publication [12].

It should be noted, that further characterisation parameters of transducers such as the impedance, the transmitting voltage response (TVR) for projectors or the receiving voltage sensitivity (RVS) for hydrophones can be derived from the complex frequency response, which represents essentially a unitless version the mentioned parameters. The unit conversion can be done by applying the reference voltage from the digitial-analog-converter, the TVR or RVS of the used reference transducer and the reference voltages from the ADC. The impedance of a transducer can be calculated from the complex frequency response as well. The main reason for our characterisation was to design equalisation filters, that correct the measured frequency response to a desired one. For that reason only the shape was of interest.

In Figure 14, a typical magnitude response is shown. It is calculated after 1 s of adaptation and shows the quick convergence of the proposed CEA method. The original magnitude, extracted from the artificial impulse response, and the magnitude based on the CEA method show no visible difference in the region of interesting frequencies between 40 and 60 kHz. However, the magnitude based on the fixed NLMS is too small, indicating a too small step size. The error between the artificial and estimated magnitudes, $|\boldsymbol{e}_{\mathrm{mag,fix}}|$ and $|\boldsymbol{e}_{\mathrm{mag,cea}}|$, is depicted for a better visibility in Figure 15. In this figure, only the interesting frequencies from 40 to 60 kHz are depicted because the chosen transmitter was designed for that bandwidth.

5 | MEASUREMENTS

To confirm the proposed algorithm, measurements were performed in the measurement tank of the WTD 71 of the German Bundeswehr on the site of the Marine Arsenal in Kiel. Since the measured impulse response $\hat{\boldsymbol{h}}$ can not be compared

to the unknown real impulse response $\boldsymbol{h}$, only an estimate of the algorithm's performance can be given. An explicitly long measurement of 25 s was performed to demonstrate, on the one hand, the improvement in convergence speed and, on the other hand, to show a better estimate by evaluating the system distance for the CEA-NLMS. A good estimator for the system distance was the in Sec. 3.6 presented evaluation on the basis of a delay time N_{T}. Because the CEA-NLMS already uses that estimate, the fixed NLMS was slightly modified to output this parameter. The convergence plot is depicted in the following in Figure 16.

At first, it is noticeable that the receive signal $\overline{y^2(n)}$, depicted in red, has lower power than the simulations. This is due to the power constraints that need to be considered on the one hand for continuously transmitting a signal and on the other hand for operating the projector in a lower depth than typically required. The constraint is projector-specific but should be around 10 % of the maximum power of the given projector. This leads to a smaller difference between hydrophone input power and error signal because the SNR is worse. Both, the error signal of the CEA-NLMS (in orange) and the fixed NLMS (in blue), bottom out at the same plateau, representing the measurement tank's noise limit. Since the real system distance cannot be calculated, the estimation of the undisturbed error is used. The estimation of the undisturbed error of the CEA-NLMS $\overline{\hat{e}^2_{\mathrm{u,cea}}(n)}$, depicted in purple, shows a better performance in contrast to the one of fixed step size NLMS $\overline{\hat{e}^2_{\mathrm{u,fix}}(n)}$, depicted in green, which forms a plateau after around 2 s. Both signals' progress might not be as smooth as the simulations, but this is probably caused by the estimation of the undisturbed error rather than the step size calculations.

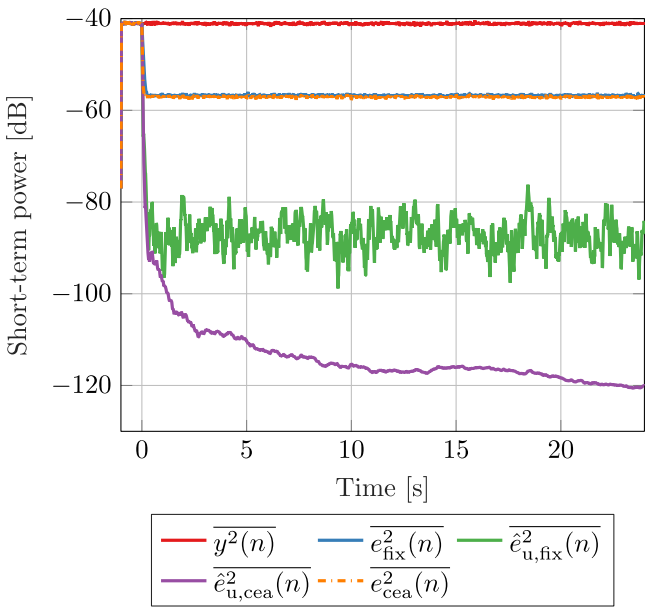

FIGURE 16 Adaptation plot for a real measurement with an explicit long measurement time of 25 s. In red is the smoothed squared receive short-term power depicted. The adaptation process starts at 0 s. In purple, the smoothed squared estimated undisturbed error of the CEA-NLMS is shown, which falls very rapidly at the beginning of the adaptation process, but does not form a plateau in contrast to the fixed normalised least mean square (NLMS), illustrated in green, which shows the limitations of a fixed step size.

6 | CONCLUSION

In this paper, all the necessary terms for understanding the NLMS algorithm were first derived and explained. Then, the undisturbed error signal estimation was discussed as the central element to determine the optimal step size. First, an estimation by subtracting measurable parameters was presented, but it was found too sensitive and inaccurate. Then, the undisturbed error signal estimation based on the theoretical adaptation behaviour of fixed (stationary) systems was explained. Using this CEA, a near-perfect estimate for the undisturbed error and; therefore, pseudo-optimal step size was obtained. This was demonstrated in simulations under different noise scenarios resulting in a near-optimal system distance. It was shown that the proposed step size control could achieve the same precision of an estimate in a quarter of the measurement time, drastically reducing the overall measurement time. Finally, the newly formed CEA-NLMS was applied to actual measurements of underwater transducers.

The described method proposes a new approach to characterise underwater transducer in terms of estimating the impulse response. For that a variable step-size algorithm was developed, that takes the possible long reverberation times of underwater measurement tanks into account. The usage of an adaptive filter also allows the estimate to be better than the SNR of the system and trough inherent quality measures. Thus, the real-time performance of the estimation can be observed and evaluated. This allows a termination of the characterisation, when the estimation quality is sufficient. The approach also achieves a major increase in convergence speed compared to a fixed step size NLMS in different SNR scenarios. This can either be used to drastically reduce the characterisation time or give a more precise estimation for the same measurement time. The first is especially useful, when a lot of similar measurements need to be done. For that reason the proposed method can be used for array characterisations or measuring the directivity of a transducer. The measured frequency response can be used to design equalisation coefficients, which can be directly applied in a second measurement to test their performance.

AUTHOR CONTRIBUTIONS

Bastian Kaulen: Conceptualisation (equal); Data curation (lead); Formal Analysis (lead); Investigation (lead); Methodology (lead); Resources (lead); Software (lead); Validation (lead); Visualisation (lead); Writing – original draft (lead); Writing – review & editing (lead). **Gerhard Schmidt**: Conceptualisation (equal); Funding acquisition (lead); Project administration (lead); Supervision (lead); Writing – review & editing (supporting).

ACKNOWLEDGEMENTS

The authors would like to thank the Bundeswehr Technical Center for Ships and Naval Weapons, Maritime Technology and Research (WTD 71), Germany for allowing us to use their measurement tank located in Kiel. Additionally, we would like to express our gratitude to Dr. A. Stoltenberg (WTD 71, Kiel, Germany) and Dr. J. Abshagen (WTD 71, Kiel, Germany) for supervising the measurements and giving advice in the physics of underwater transducers.

Open Access funding enabled and organized by Projekt DEAL.

CONFLICT OF INTEREST STATEMENT

No conflict of interest to disclose by the authors.

DATA AVAILABILITY STATEMENT

Research data are not shared.

ORCID

Bastian Kaulen https://orcid.org/0000-0003-1610-4077
Gerhard Schmidt https://orcid.org/0000-0002-6128-4831

REFERENCES

1. Istepanian, R.S., Stojanovic, M.: Underwater Acoustic Digital Signal Processing and Communication Systems. Kluwer Academic PublishersUSA (2002)
2. Ainslie, M.: Principles of Sonar Performance Modelling (2010)
3. Peyvandi, H., et al.: SONAR Systems and Underwater Signal Processing: Classic and Modern Approaches (2011)
4. Li, Q.: Digital Sonar Design in Underwater Acoustics (2012)
5. Bar-Shalom, Y., Li, X., Kirubarajan, T.: Estimation with Applications to Tracking and Navigation: Theory. algorithms and software (2001)
6. Robinson, S.P.: Review of Methods for Low Frequency Transducer Calibration in Reverberant Tanks (1999)
7. Cochard, N., et al.: Underwater acoustic noise measurement in test tanks. IEEE J. Ocean. Eng. 25(4), 516–522 (2000). https://doi.org/10.1109/48.895359
8. Hazelwood, R., Robinson, S.: Underwater Acoustic Power Measurements in Reverberant Fields, pp. 1–6 (2007)
9. Schulze, S.: Echo reduction in hydro-acoustic measurements. In: Underwater Acoustics Conference and Exhibition vol. 3, pp. 273–280 (2015)
10. Farina, A.: Simultaneous Measurement of Impulse Response and Distortion with a Swept-Sine Technique, pp. 11 (2000)
11. Gemba, K., Nosal, E.-M., Reed, T.: Estimating and removing colorations from the deconvolved impulse response of an underwater acoustic channel. J. Acoust. Soc. Am. 141(1), EL6–EL10 (2017). https://doi.org/10.1121/1.4973311
12. Kaulen, B., et al.: Entwurf und Implementierung einer schnellen Frequenzgangmessung und automatischer Entzerrung von akustischen Schallwandlern. In: Processing DAGA (2022). March 2022
13. Hänsler, E., Schmidt, G.: Algorithms for Adaptive Filters. John Wiley & Sons, Ltd (2004)
14. Hänsler, E., Schmidt, G.: Control of LMS-type Adaptive Filters, pp. 175–240 (2005)
15. Haykin, S., Haykin, S.: Adaptive Filter Theory. Pearson (2014)
16. Antweiler, C., Grunwald, J., Quack, H.: Approximation of optimal step size control for acoustic echo cancellation. In: 1997 IEEE International Conference on Acoustics, Speech, and Signal Processing, vol. 1, pp. 295–298 (1997)
17. Benesty, J., et al.: A nonparametric vss nlms algorithm. Signal Process. Lett. IEEE 13(10), 581–584 (2006). https://doi.org/10.1109/lsp.2006.876323
18. Iqbal, M.A., Grant, S.L.: Novel variable step size nlms algorithms for echo cancellation. In: 2008 IEEE International Conference on Acoustics, Speech and Signal Processing, pp. 241–244 (2008)
19. Ciochină, S., et al.: An Optimized Nlms Algorithm for Acoustic Echo Cancellation, pp. 1–4 (2015)
20. Ciochină, S., Paleologu, C., Benesty, J.: An optimized nlms algorithm for system identification. Signal Process. 118, 115–121 (2016). https://doi.org/10.1016/j.sigpro.2015.06.016
21. Reson, T.M.: Datasheet Reson Tc4014 (2016). Online www.teledynemarine.com/Lists/Downloads/TC4014%20product%20leaflet.pdf. accessed 25 July 2022
22. Rebbe, K., Wisch, T., Schmidt, G.: Recursive Computation of Signal Vector Norms (2017). Online https://dss-kiel.de/index.php/teaching/red-main/red-recursive-computation-of-signal-vector-norms. accessed 25 July 2022
23. Gomez-Alfageme, J., Bote, J., Blanco-Martin, E.: New Measurement Methods for Anechoic Chamber Characterization, vol. 3, pp. 01 (2012)
24. Samarasinghe, P.N., et al.: Estimating the direct-to-reverberant energy ratio using a spherical harmonics-based spatial correlation model. IEEE/ACM Trans. Audio, Speech and Lang. Proc. 25(2), 310–319 (2017). https://doi.org/10.1109/taslp.2016.2633811
25. Yamamoto, S., Kitayama, S.: An adaptive echo canceller with variable step gain method. In: Nstitute of Electronics Communication Engineers of Japan Transactions Section E English, vol. 65, pp. 1–8. (1982)
26. Schultheiß, U.: Über die Adaption eines Kompensators für akustische Echos. Düsseldorf: VDI-Verl. (1988)

How to cite this article: Kaulen, B., Schmidt, G.: Fast and precise underwater transducer characterisation utilising adaptive system identification. IET Radar Sonar Navig. 17(7), 1160–1174 (2023). https://doi.org/10.1049/rsn2.12409